Theory of the alkali-metal chemisorption on metal surfaces

H. Ishida
Institute for Solid State Physics, University of Tokyo, Roppongi, Minato-ku, Tokyo 106, Japan
(Received 19 February 1988; revised manuscript received 8 June 1988)

The electronic structure of the alkali-metal adatom on metal surfaces is studied by a first-principles method as a function of adatom coverage (Θ). We employ "jellium" as a high-density metal substrate to make a continuous change of Θ possible. Although the characteristic variation of the work function with Θ is reproduced well by the present calculation, its mechanism is different from a widely accepted mechanism in which the adatom electronic structure is assumed to change from ionic to neutral with increasing Θ by the depolarization shift. The charge redistribution $\delta\rho(\mathbf{r},\Theta)$ that lowers the work function deviates far from the point-charge-transfer model, and the electrostatic potential change at adatom sites due to $\delta\rho(\mathbf{r},\Theta)$ depends very little on Θ. Accordingly, the adatom valence density of states shows no downward shift with increasing Θ. The adatom region is essentially neutral, even at low Θ. The bonding-antibonding boundary in the bond-order density of the adatom-substrate bond coincides well with the Fermi level at low Θ, indicating a formation of a metallic bond by the maximum use of bonding states even at low Θ. The close similarity between the calculated bond-order and dipole densities as a function of the one-electron energy implies that the adatom polarization due to the hybridization of adatom and substrate orbitals plays an important role for the adatom dipole and its Θ dependence even at low Θ. The decrease of the adatom dipole is explained by a weakening of the adatom-substrate bonding as well as a significant decrease in the dipole matrix elements with increasing Θ.

I. INTRODUCTION

Alkali-metal adsorption on metal surfaces has been studied for a long time as one of the simplest chemisorption systems showing various electronic properties. In 1923, Kingdon and Langmuir[1] discovered that the electron-emission rate of W, Ni, and Mo filaments is greatly increased by the Cs adlayer, which implied a considerable lowering of the work function. Based on a classical picture, the result was explained as follows: As the ionization energy of Cs ($I=3.89$ eV) is smaller than the work function of the substrates ($\Phi\sim4.5$ eV), Cs is ionized on the surface, and the resultant dipole layer formed by Cs^+ and its negative image charge lowers the potential barrier of an outgoing electron. Taylor and Langmuir[2] studied the rate of atom, ion, and electron emissions of Cs on W as functions of coverage (Θ) and temperature and showed that the work function takes a minimum value before reaching a saturation coverage. Afterward, similar variations of the work function with Θ, i.e., an initial rapid lowering followed by a minimum and a subsequent small rise toward a saturation value, have been observed in many studies of the alkali-metal chemisorption.[3-5] Because of its relevance to cathode technology, most of the experiments employed transition metals as substrates. Nevertheless, the same behavior is observed on simple metals such as Be and Al,[6-8] and even on semiconductors.[9]

Since the work-function lowering $\Delta\Phi(\Theta)$ is proportional to $d(\Theta)$ [$d(\Theta)$ denotes the induced moment per an adatom] multiplied by Θ, its characteristic variation indicates a rapid decrease of $d(\Theta)$ with increasing Θ. The first quantum-mechanical treatment of the problem was given by Gurney[10] in 1935. He pointed out that the alkali-metal valence s level suffers a lifetime broadening on metal substrates, and thus even if its center is located above the Fermi level (E_F) the adatom ionization is not complete. Provided adatoms are chemisorbed essentially as ions at lower Θ, the decrease of $d(\Theta)$ with increasing Θ may be interpreted as indicating smaller ionicity of adatoms. Gurney gave a plausible explanation of their neutralization with increasing Θ by invoking a downward shift of the s resonance which may be caused by a potential lowering of adatom sites due to dipole fields of the other adatoms (depolarization field). The Θ dependence of the adatom s resonance proposed by Gurney is schematically shown in Fig. 1. Since the work of Gurney, the ionic-neutral (metallic) change of the alkali-metal adatoms with increasing Θ has been believed for more than half a century as a basic concept in alkali-metal chemisorption.

Recently, there appeared some works which casted a doubt upon the validity of Gurney's treatment. The metastable-He deexcitation spectroscopy (MDS) experiment by Woratschek *et al.*[11] for K/Cu(110) suggested that the decrease of $d(\Theta)$ with increasing Θ might not be directly associated with the occupation of the K 4s resonance. Soukiassian *et al.*[12] and Tochihara *et al.*[13] measured the binding energy of Cs 5p core orbitals as a function of Cs coverage on W(001) and Si(111), respectively. The measured Cs 5p level shifted very little with Θ, which implied that the depolarization field might be absent at adatom sites in real systems. On the theoretical side, Wimmer *et al.*[14] performed a first-principles electronic-structure calculation for Cs/W(001) and concluded that the work-function lowering is caused by the

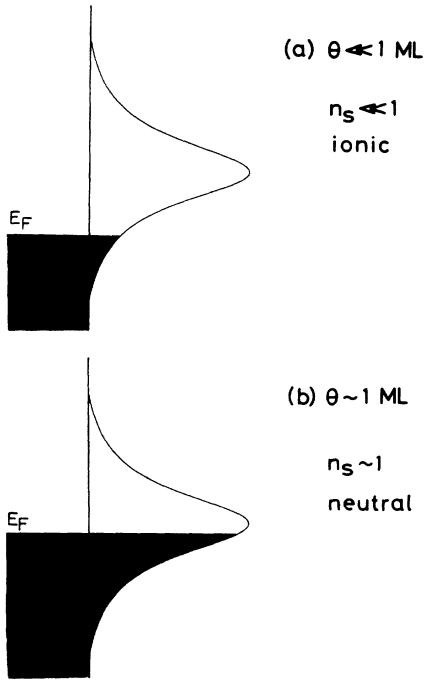

FIG. 1. Schematic energy diagram of the alkali-metal adatom s resonance originally proposed by Gurney (Ref. 10) at (a) the low-Θ and (b) the high-Θ limit. ML denotes monolayers.

polarization of Cs due to the hybridization of Cs $6s$ and W $5d$ rather than Cs ionization. However, as the calculation was done at the high-Θ limiting assuming a $c(2\times2)$ structure ($\Theta=\frac{1}{2}$ in units of W layers) for Cs, it was not clear whether their conclusion is valid even at low Θ, where it is believed that adatoms become much more ionic.

The purpose of the present paper is to help resolve the above-mentioned controversial subject and to provide a more correct picture for alkali-metal adsorption. We will perform first-principles electronic-structure calculations of alkali-metal-covered metal surfaces, with a range of Θ values, and clarify the nature of adatom-substrate bonding and the origin of the adatom dipole as a function of Θ. (A short paper on parts of this work has been already published.[15]) To date, electronic-structure calculations of the alkali-metal overlayers on metal and semiconductors surfaces have been restricted at the high-Θ limit because the two-dimensional periodicity of substrates hinders continuous change of Θ and also the amount of labor required increases rapidly with decreasing Θ.[14,16–19] In order to evade mainly the former difficulty, we employ "jellium" as a substrate, where discrete ion cores of the substrate are smeared out into a uniform positive background charge. Various phenomena observed on alkali-metal-covered metal surfaces are independent of the detailed characteristics of substrates, such as the number of d electrons and geometry of surface atoms. Therefore the choice of jellium as the substrate seems quite acceptable in order to extract the essence of the phenomena. Though the details of adsorbate (s)–substrate (d) hybridization are omitted from the electronic structure when the substrate is modeled by jellium, for evaluating quantities like the change in work function, and induced changes in dipole moment, which depend on the distribution of charge only in an average way, the use of jellium is adequate. Furthermore, because currently there has been some controversy concerning the evaluation of even these quantities using considerably more simplified ionic models (e.g., using the Newns-Anderson model) than the first-principles approach used in the current work, the use of jellium for the substrate provides a useful starting point for clearing up much of the controversy associated with alkali-metal adsorption. This is especially so because the results from the current work reveal that even when d electrons are entirely omitted from the description considerably greater covalency is found than was envisioned in the ionic model of Gurney. There is a restriction in the lowest value of Θ achieved in the present calculation because of the limit of computer capacity. Nevertheless, chemisorption of a single alkali-metal atom on jellium surfaces was studied by Lang and Williams,[20] which corresponds to the limit of $\Theta\rightarrow0$ in the present calculation. By comparing the calculated result with theirs, we can check the accuracy of the present calculation at low Θ.

The plan of the present paper is as follows. In Sec. II we briefly review phenomenological models advanced so far for the study of alkali-metal adsorption and discuss unreliable assumptions involved in them. In the latter half of Sec. II some general discussions of the adatom dipole moment are given for the sake of convenience in the later sections. The present calculation is based on the local-density-functional theory combined with the norm-conserving pseudopotential. The calculational method and overlayer models are summarized in Sec. III. Section IV is the main part of the present paper and is devoted to the results and discussions of the present calculation. Finally, summary and conclusions are given in Sec. V. Throughout the paper the atomic units, $m=1$, $e=1$, $\hbar=1$, are used. The units of length and energy are 0.529 Å and 27.2 eV, respectively.

II. CRITICAL REVIEW OF PHENOMENOLOGICAL MODELS

In 1971 Lang[21] presented a simplified model of the alkali-metal adsorption, where the adatom ion cores were modeled by a thin jellium slab adsorbed on a high-density jellium surface. The thickness of the slab was fixed and the increase in the number of ion cores was simulated by changing the density of the slab as being proportional to Θ. The rapid decrease of the work function at lower Θ, as well as the presence of a minimum, was reproduced well by the model, which became the impetus for its subsequent extension.[22–25] However, at least for low Θ, the success of the model does not necessarily mean that the physics involved in the model is realistic. To begin with, the idea of modeling the alkali-metal ion cores by the jellium is based on the fact that *bulk* alkali metals are the best examples of free-electron metals. However, the applicability of such a model is justified only when the orbital overlap between neighboring atoms is large enough

to lead to a large valence-band width. With decreasing Θ, the overlayer tends to be a set of isolated atoms. In this limit, each electron is accommodated in the s orbital of an ion core with a binding energy of 4–5 eV. On the other hand, if the overlayer is represented by the jellium, the electron binding energy tends to zero at the low-Θ limit. In this case it is not surprising that electrons in the overlayer flow to the substrate, forming a dipole layer which lowers the work function. However, actually, the phenomenon which must be clarified by theory is the dipole inducement due to the interaction of metal substrates with electrons with a (4–5)-eV binding energy, and *not* with those with *zero* binding energy. The unrealistic nature of the model at low Θ may be disclosed more clearly if one thinks of a situation in which the substrate the adsorbate are interchanged; for example, adsorption of Al atoms on a bulk Na surface. Since Al is also a good example of a free-electron metal, the jellium approximation for the Al layer would be no worse than for the alkali metals. Then the model would again result in a rapid *decrease* of the work function at low Al Θ. However, Al actually induces a negative dipole on Na, which results in the *increase* of the work function.[26] Hence, the jellium model for the overlayer breaks down in this case.

The second model[27–32] employs the Newns-Anderson Hamiltonian,[33,34]

$$H=\sum_{k,\sigma}\varepsilon_k C_{k\sigma}^{\dagger}C_{k\sigma}+\varepsilon_s(\Theta)\sum_{\sigma}C_{s\sigma}^{\dagger}C_{s\sigma}+\sum_{k,\sigma}(V_{ks}C_{k\sigma}^{\dagger}C_{s\sigma}+\text{H.c.}) , \tag{2.1}$$

where we follow the standard notation. The most important parameter in this model is the effective energy of the adatom s level,

$$\varepsilon_s(\Theta)=-I+\frac{e^2}{4D}+\varepsilon_{\text{dep}}(\Theta) , \tag{2.2}$$

where I is the first ionization energy of an alkali-metal atom, and the latter two terms designate level shifts due to the image effect and depolarization field. Since the ionization energies of alkali-metal atoms are 5.39, 5.14, 4.34, 4.18, and 3.89 eV for Li, Na, K, Rb, and Cs, respectively, while the work function of metal substrates is typically $\sim$4 eV, adatom ionization is hardly expected from the comparison of these two parameters. In fact, the crucial assumption required for the adatom ionization is the upward shift of the s level by the image term $e^2/4D$, whose origin is the surface relaxation by virtual excitations of the surface plasmon. Hewson and Newns[35] showed that such a treatment is justified only in the case

$$\Delta(\varepsilon)\ll\omega_s , \tag{2.3}$$

where

$$\Delta(\varepsilon)=\pi\sum_k |V_{ks}|^2\delta(\varepsilon-\varepsilon_k) , \tag{2.4}$$

and ω_s is the surface-plasmon frequency. Since alkali-metal adatoms are adsorbed at a position where their orbitals entirely overlap with substrate ones, the interaction between them might not be so weak as that satisfying Eq. (2.3). Furthermore, the classical expression $e^2/4D$ for the relaxation energy is not valid when adatom orbitals overlap with the substrate image plane.

The depolarization energy $\varepsilon_{\text{dep}}(\Theta)$, which ensures a downward shift of the s level, is expressed as

$$\varepsilon_{\text{dep}}(\Theta)=-\sum_i[|\mathbf{x}_i|^{-1}-(\mathbf{x}_i^2+D^2)^{-1/2}]Q(\Theta) , \tag{2.5}$$

where the summation is taken over all adatom sites, excluding that described in Eq. (2.1), and $Q(\Theta)$ is the charge transfer from an adatom to the substrate. Equation (2.5) is based on a classical picture that a point charge $Q(\Theta)$ is transferred from the center of adatoms to substrate atoms with perpendicular interval D. However, in contrast to the classical picture the increase and decrease of the electron density in real systems appear in the interface and vacuum sides of an adatom, respectively (see Fig. 5). The electrostatic potential is surely lowered on the vacuum side of an adatom, whereas it is almost independent of Θ at adatom sites due to the efficient screening effect of high-density metal substrates. Therefore, one cannot expect a large depolarization energy such as $\sim$1 eV, which is necessary for the neutralization of adatoms at higher Θ.

Why is it then necessary to introduce the above-mentioned unreliable assumptions when working on the Newns-Anderson model? This is because $d(\Theta)$ is evaluated by the formula[27–30]

$$d(\Theta)=D[1-n_a(\Theta)]=D\left[1-\sum_{\sigma}\langle C_{s\sigma}^{\dagger}C_{s\sigma}\rangle\right] . \tag{2.6}$$

Then in order to explain a large dipole at low Θ and its rapid decrease with increasing Θ, it is necessarily required that $n_a(\Theta)\ll 1$ at low Θ, while $n_a(\Theta)\sim 1$ at higher Θ. The upward shift of the s level by the image effect and its subsequent downward shift by the depolarization field are convenient devices which ensure the above Θ dependence of the s-level occupation. However, it is not correct to consider that Eq. (2.6) alone contributes to $d(\Theta)$. A more general expression for $d(\Theta)$ should be derived in order to make the situation clearer. First, we define the dipole density as

$$\mu(\Theta,\varepsilon)=-\frac{1}{\pi}\int d\mathbf{r}\, z\,\text{Im}G(\mathbf{r},\mathbf{r},\varepsilon+i\delta) , \tag{2.7}$$

where $G(\mathbf{r},\mathbf{r},\varepsilon+i\delta)$ is the Green function $(\varepsilon+i\delta-H)^{-1}$ (δ is an infinitesimal positive number). The z axis is the surface normal pointing to the vacuum and $z=0$ is understood to coincide with the adatom plane. $\mu(\Theta,\varepsilon)$ is related to $d(\Theta)$ by

$$d(\Theta)=\frac{1}{N}\int_{\varepsilon\le E_F}d\varepsilon[\mu(\Theta,\varepsilon)-\mu(\Theta=0,\varepsilon)] , \tag{2.8}$$

where N is the number of adatoms. Unless the origin of the z axis is at the adatom plane, $\mu(\Theta,\varepsilon)$ corresponding to isolated adatoms must be subtracted from Eq. (2.8) for evaluating $d(\Theta)$. Let us denote the basis functions for the adatom s and substrate states as $\varphi_\alpha(\mathbf{r})$, and $\varphi_\beta(\mathbf{r})$, respectively. They are assumed to be normalized and orthogonal with one another. Then neglecting the adatom-

adatom as well as substrate-substrate mixing, $\mu(\Theta,\varepsilon)$ is written as

$$\mu(\Theta,\varepsilon)=-\frac{1}{\pi}\left[\sum_{\alpha}\mu_{\alpha\alpha}\mathrm{Im}G_{\alpha\alpha}(\varepsilon+i\delta)+\sum_{\beta}\mu_{\beta\beta}\mathrm{Im}G_{\beta\beta}(\varepsilon+i\delta)+\sum_{\alpha,\beta}[\mu_{\beta\alpha}\mathrm{Im}G_{\alpha\beta}(\varepsilon+i\delta)+\text{c.c.}]\right], \quad (2.9)$$

where the dipole matrix element between the i and j states is defined as

$$\mu_{ij}=\int d\mathbf{r}\, z\varphi_i^*(\mathbf{r})\varphi_j(\mathbf{r}) . \quad (2.10)$$

The first term in Eq. (2.9) vanishes because $\mu_{\alpha\alpha}=0$ due to the symmetry of $\varphi_\alpha(\mathbf{r})$ about the plane $z=0$. The total density of states (DOS) of the system $\rho(\Theta,\varepsilon)$ is written in a similar way as

$$\rho(\Theta,\varepsilon)=-\frac{1}{\pi}\left[\sum_{\alpha}\mathrm{Im}G_{\alpha\alpha}(\varepsilon+i\delta)+\sum_{\beta}\mathrm{Im}G_{\beta\beta}(\varepsilon+i\delta)\right] . \quad (2.11)$$

Here the mixing term between adatom and substrate states does not appear because of the orthogonality of basis functions. Let us ignore the β dependence of $\mu_{\beta\beta}$ and replace it by a single parameter D. Then, from Eqs. (2.9) and (2.11), $\mu(\Theta,\varepsilon)$ is divided into two terms as

$$\mu(\Theta,\varepsilon)=\mu_{\mathrm{CT}}(\Theta,\varepsilon)+\mu_{\mathrm{hyb}}(\Theta,\varepsilon) , \quad (2.12)$$

where

$$\mu_{\mathrm{CT}}(\Theta,\varepsilon)=D\left[\rho(\Theta,\varepsilon)+\frac{1}{\pi}\sum_{\alpha}\mathrm{Im}G_{\alpha\alpha}(\varepsilon+i\delta)\right] \quad (2.13)$$

and

$$\mu_{\mathrm{hyb}}(\Theta,\varepsilon)=-\frac{1}{\pi}\sum_{\alpha,\beta}[\mu_{\beta\alpha}\mathrm{Im}G_{\alpha\beta}(\varepsilon+i\delta)+\text{c.c.}] . \quad (2.14)$$

By using the relations

$$\int_{\varepsilon\le E_F}d\varepsilon[\rho(\Theta,\varepsilon)-\rho(\Theta=0,\varepsilon)]=N ,$$
$$\int_{\varepsilon\le E_F}d\varepsilon-\frac{1}{\pi}\sum_{\alpha}\mathrm{Im}G_{\alpha\alpha}(\varepsilon+i\delta)=Nn_a(\Theta) , \quad (2.15)$$

the induced dipole by Eq. (2.13) is reduced to $D[1-n_a(\Theta)]$, which coincides with the familiar expression (2.6), giving a contribution of the charge transfer (CT). As seen from the definition, it originates from the increase in the DOS of substrate states in the surface region by perturbation. There may be ambiguity in the definition of the concept "charge transfer." In the present paper it is used in a narrow sense to denote the above-mentioned change in the occupation of the adatom orbitals and rigorously distinguished from the term "charged redistribution," which includes hybridization effects. On the other hand, the other contribution, Eq. (2.14), originates from polarization of adatoms by the hybridization of adatom s and substrate states, which was ignored completely in previous model calculations. This term vanishes, for example, in case of homonuclear diatomic molecules. However, for alkali-metal adatoms on metals with a much lower symmetry, there is no reason to believe that this off-diagonal contribution to the dipole is dominated by the conventional diagonal charge-transfer term. In fact, at a high-Θ limit Wimmer *et al.*[14] demonstrated that the work function is lowered by the hybridization of Cs 6*s* and W 5*d* for Cs/W(001).

In the first-principles electronic-structure calculations it is impossible to divide in a definite way the calculated total dipole density into these two contributions, because the basis functions for substrate and adatom states cannot be chosen uniquely. Nevertheless, from the energy dependence of $\mu(\Theta,\varepsilon)$ it seems possible to postulate the origin of the dipole density in a qualitative manner. From the definition, $\mu_{\mathrm{CT}}(\Theta,\varepsilon)$ has a positive sign as a function of energy. On the other hand, the dipole density due to the hybridization, $\mu_{\mathrm{hyb}}(\Theta,\varepsilon)$, shows a characteristic energy dependence. The off-diagonal Green function $G_{\alpha\beta}(\varepsilon+i\delta)$ is given as[36]

$$G_{\alpha\beta}(\varepsilon+i\delta)=G_{\alpha\alpha}(\varepsilon+i\delta)V_{\alpha\beta}\frac{1}{\varepsilon+i\delta-\varepsilon_\beta} , \quad (2.16)$$

where

$$G_{\alpha\alpha}(\varepsilon+i\delta)=\frac{1}{\varepsilon-\varepsilon_\alpha-\Delta_\alpha(\varepsilon)+i\Gamma_\alpha(\varepsilon)} . \quad (2.17)$$

Here, ε_α, ε_β, and $V_{\alpha\beta}$ are the diagonal and off-diagonal matrix elements of the Hamiltonian. If the interaction among neighboring adatom s orbitals is small, the energy shift $\Delta_\alpha(\varepsilon)$ and width $\Gamma_\alpha(\varepsilon)$ of the s resonance may be approximately given by

$$\Delta_\alpha(\varepsilon)-i\Gamma_\alpha(\varepsilon)=\sum_{\beta}\frac{|V_{\alpha\beta}|^2}{\varepsilon+i\delta-\varepsilon_\beta} . \quad (2.18)$$

From Eqs. (2.14), (2.16), and (2.17), we have

$$\mu_{\mathrm{hyb}}(\Theta,\varepsilon)=\sum_{\alpha}\frac{B_\alpha(\varepsilon)}{\pi}\times\frac{\varepsilon-\varepsilon_\alpha-\Delta_\alpha(\varepsilon)+[A_\alpha(\varepsilon)/B_\alpha(\varepsilon)]\Gamma_\alpha(\varepsilon)}{[\varepsilon-\varepsilon_\alpha-\Delta_\alpha(\varepsilon)]^2+\Gamma_\alpha(\varepsilon)^2}+\text{c.c.} \quad (2.19)$$

In the above $A_\alpha(\varepsilon)$ and $B_\alpha(\varepsilon)$ are defined as

$$A_\alpha(\varepsilon)=\mathrm{P}\sum_{\beta}\frac{V_{\alpha\beta}\mu_{\beta\alpha}}{\varepsilon-\varepsilon_\beta} , \quad (2.20)$$

$$B_\alpha(\varepsilon)=\pi\sum_{\beta}V_{\alpha\beta}\mu_{\beta\alpha}\delta(\varepsilon-\varepsilon_\beta) , \quad (2.21)$$

where P denotes the principal part. Since the energy dependence of $\Delta_\alpha(\varepsilon)$, $\Gamma_\alpha(\varepsilon)$, $A_\alpha(\varepsilon)$, and $B_\alpha(\varepsilon)$ is not large unless substrate bands are narrow, they may be assumed to be energy independent. Then, Eq. (2.19) shows that $\mu_{\rm hyb}(\Theta,\varepsilon)$ rapidly changes its sign at

$$\varepsilon=\varepsilon_\alpha+\Delta_\alpha-(A_\alpha/B_\alpha)\Gamma_\alpha\ . \tag{2.22}$$

This boundary is shifted from the center of the s resonance by the term $(A_\alpha/B_\alpha)\Gamma_\alpha$. If the β dependence of the matrix elements $V_{\alpha\beta}\mu_{\beta\alpha}$ is neglected, and the substrate band has an energy-independent DOS, A_α vanishes and the boundary coincides exactly with the resonance peak.

Another quantity closely related with $\mu_{\rm hyb}(\Theta,\varepsilon)$ is the bond-order density, defined by

$$\begin{aligned}\beta(\Theta,\varepsilon)&=\sum_n[\psi_n(\mathbf{r}_1)]^*\psi_n(\mathbf{r}_2)\delta(\varepsilon-\varepsilon_n)+\text{c.c.}\\&=-\frac{1}{\pi}\sum_{\alpha,\beta}[\varphi_\beta(\mathbf{r}_1)]^*\varphi_\alpha(\mathbf{r}_2)\text{Im}G_{\alpha\beta}(\varepsilon+i\delta)+\text{c.c.}\ ,\end{aligned} \tag{2.23}$$

where ε_n and $\psi_n(\mathbf{r})$ are the energy and wave function of one-electron states, and $\mathbf{r}_1$ and $\mathbf{r}_2$ are assumed in the substrate and adatom regions, respectively. It may be used as a measure of covalency in the adatom-substrate bond. $\beta(\Theta,\varepsilon)$ is given by the same expression, Eq. (2.19), if $\mu_{\beta\alpha}$ is replaced by $[\varphi_\beta(\mathbf{r}_1)]^*\varphi_\alpha(\mathbf{r}_2)$ in evaluating $A_\alpha(\varepsilon)$ and $B_\alpha(\varepsilon)$ in Eqs. (2.20) and (2.21). Thus, $\mu_{\rm hyb}(\Theta,\varepsilon)$ and $\beta(\Theta,\varepsilon)$ show a similar energy dependent. If the calculated total dipole density behaves in a way similar to the bond-order density as a function of energy, one may infer that $d(\Theta)$ comes mainly from the hybridization. The positive and negative parts of the bond-order density correspond to the bonding and antibonding states, respectively. The bonding-antibonding (B-A) boundary coincides with the center of the resonance peak if $(A_\alpha/B_\alpha)\Gamma_\alpha$ is small. Indeed, for a single adatom on high-density jellium, Lang and Williams[20] showed that the lower and upper halves of an adatom resonance have bonding and antibonding characteristics, respectively. The charge accumulation (depletion) in the interface region in the bonding (antibonding) states is the origin of the hybridization-induced dipole density and its rapid change of sign near the B-A boundary around a center of the resonant peak.

The concept of the adatom polarization due to hybridization must be strictly distinguished from that of charge transfer. In Fig. 2 the induced dipole moments due to the charge transfer, $d_{\rm CT}(\Theta)$, and hybridization, $d_{\rm hyb}(\Theta)$, are shown schematically as a function of E_F relative to the center of the s resonance. $d_{\rm CT}(\Theta)$ disappears when E_F is located at the center of the s resonance, whereas $d_{\rm hyb}(\Theta)$ becomes the largest by the maximum use of bonding states in this case. Since the work function of high-density metal substrates ($\Phi\sim4$–5 eV) is comparable to ionization energies of alkali-metal atoms, this might surely be the case in real systems.

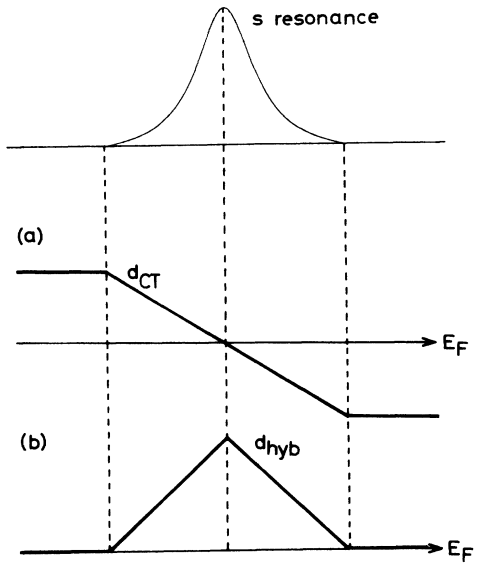

FIG. 2. (a) Charge-transfer- and (b) hybridization-induced dipole moments as a function of the substrate Fermi level (E_F) relative to the center of the alkali-metal adatom s resonance.

III. CALCULATIONAL METHOD AND OVERLAYER MODEL

The *ab initio* calculation in the present work is performed within the local-density approximation in the density-functional theory.[37,38] The sources of the external field are the jellium substrate and ion cores of alkali-metal adatoms. The adatom ion cores are represented by the nonlocal norm-conserving pseudopotential of Bachelet, Hamann, and Schlüter.[39] The surface-electronic-structure calculation is performed by utilizing a conventional repeating-slab geometry in which the semi-infinite surface is replaced by a thin slab and the slab geometry is repeated periodically in the surface-normal direction. The one-electron wave function is expanded by the plane-wave basis set, which is fitted for the description of a minute difference in the electron density necessary for the accurate evaluation of the work function of the order of 0.1 eV. The cutoff energy for the plane-wave bases is 6.5 Ry in the present calculation, which is sufficiently large for the alkali metals and jellium substrate.

Because of the negligible interaction of neighboring slabs, the diagonalizing of the seqular equation is necessary only in the two-dimensional Brillouin zone, where the z (surface normal) component of the wave vector is zero. For Na/jellium at $\Theta=1$ (see the next section as for the definition of Θ), its square Brillouin zone is divided into 8×8 meshes. A similar mesh density is used for other coverages. By virtue of mirror symmetry with respect to the center plane of the substrate, the plane waves can be classified into even and odd bases and separatively diagonalized. The number of plane-wave bases exceeds 4500 in the largest system in the present calculation. No perturbative approaches are used and all the bases are diagonalized exactly.

Once the seqular equation is solved in the independent

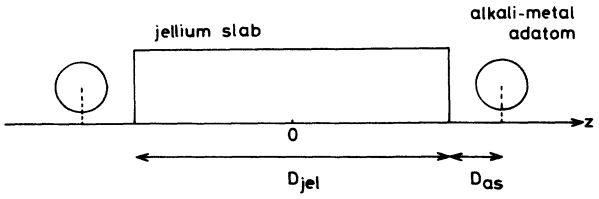

FIG. 3. Slab geometry used for the electronic-structure calculation of the alkali-metal overlayers on the jellium surface.

points in the Brillouin zone, the output charge density is constructed. The k-space integration is done with the tetrahedron method.[40] The initial input charge is the superposed density of the bare substrate and unsupported overlayer. The mixing rate of input and output charge densities for the next iteration is typically $\sim 5\%$. The iteration procedure is continued until the difference between the input and output surface dipole layers converges less than 0.1 eV. The calculated total energy converges much faster than the potential energy and the convergence of less than 1 meV is easily attained.

Figure 3 shows the model geometry used for the study of the alkali-metal adsorption on the jellium surface. The alkali-metal atoms are adsorbed on both sides of the substrate to preserve symmetry. Most of the calculations are done employing Na as the adsorbate, but the effect of different alkali-metal adspecies will be also examined. So as to simulate the adsorption on high-density metal substrates, the jellium density is chosen as $n_{jel}=0.0267$ a.u. ($r_s=2.1$ a.u.), which corresponds to the bulk electron density of Al. D_{jel} and A_z (the period in the z direction) are chosen as 16 and 48 a.u., respectively, by which the work function of the semi-infinite jellium, 3.8 eV (Ref. 41), is reproduced. The two-dimensional structure of the overlayer is entirely at one's disposal as far as the translational symmetry is kept. In the present work the overlayers are assumed to form a square lattice with a lattice constant $a_{\parallel}$, and Θ is controlled by changing $a_{\parallel}$. Because of the extended nature of the s orbital, as well as the lack of p electrons, which may result in polarized sp orbitals, the different choice of the overlayer structure would not change qualitative aspects of the results. Another important parameter is the distance between the adsorbate and substrate, D_{as}. Wimmer *et al.*[14] treated D_{as} as an adjustable parameter and examined the D_{as} dependence of the work function for Cs/W(001) ($\Theta=\frac{1}{2}$). [All values of Θ are in monolayers (ML).] In the present calculation D_{as} is determined from the minimization of the calculated total energy for higher Θ. It will be shown that the relaxation of D_{as} is not so large and of an order of 0.1 a.u. Within the variation of D_{as} in this order, the change of the work function is small. Thus, D_{as} is fixed for lower Θ in order to save the computational work.

IV. RESULTS AND DISCUSSION

The electronic-structure calculations of the Na layers on the high-density jellium ($r_s=2.1$ a.u.) surface are done for five coverages. The lattice constant $a_{\parallel}$ for the highest Θ is chosen as 8.0 a.u. Just for the sake of convenience, this coverage is defined as $\Theta=1$. But it is not necessarily meant that $\Theta=1$ corresponds to the full coverage in experimental systems. Since the nearest Na-Na distance is 6.6 a.u. in bulk Na, $\Theta=1$ may roughly correspond to ~ 60–70% of the full coverage. The other calculations are done for $\Theta=\frac{3}{4}$, $\frac{1}{2}$, $\frac{1}{3}$, and $\frac{1}{5}$, where $a_{\parallel}=9.238$, 11.314, 13.856, and 17.888 a.u., respectively.

The total-energy minimization was done in determining the adatom-jellium distance D_{as} for $\Theta=\frac{1}{2}$, $\frac{3}{4}$, and 1. The calculated energy minimum points are $D_{as}=2.9$, 3.0, and 3.1 a.u. for $\Theta=\frac{1}{2}$, $\frac{3}{4}$, and 1, respectively. The vibrational frequency of the stretching motion of Na in the surface-normal direction is estimated as ~ 17 meV from the curvature of the total-energy curve as a function of D_{as} at the minimum point. The frequency is found to decrease slightly with increasing Θ. Because the number of sampling points for D_{as} was not taken so densely, we will not discuss vibrational properties of the overlayer in more detail in the present work, though they are quite interesting. Within the variation of D_{as} of an order of 0.1 a.u., the resultant work-function change is only of the order of 0.01 eV. Thus, in order to save computational efforts, the D_{as} are assumed to be 2.9 a.u. for $\Theta=\frac{1}{5}$ and $\frac{1}{3}$. The small outward relaxation of Na with increasing Θ reflects the weakening of the Na-jellium bond with increasing Θ, as will be discussed later. Muscat and Batra[29] proposed that the outward relaxation of the overlayer with increasing Θ is essential in reproducing the observed work-function variation. They required a large D_{as} relaxation of ~ 1 a.u. for fitting their results to experimental work-function curves. However, such a value seems somewhat too large, even with different choices of substrates and adatoms, and the disagreement with experiments should be ascribed to their use of a simplified model based on the Newns-Anderson Hamiltonian.

A. Charge density and difference charge

The upper panels of Fig. 4 show the calculated electron charge densities on a vertical-cut plane passing Na atoms at every interval of $a_{\parallel}$ for $\Theta=1$ and $\frac{1}{3}$. The Na atoms and jellium edges are shown by the solid circles and arrows, respectively. Because of the pseudopotential calculation the charge density assumes a minimum at Na sites. The ample magnitude of the electron density in the midregion of the neighboring Na atoms at $\Theta=1$ indicates that the Na layer has a metallic character at this coverage. However, it is not meant that the overlayer is a two-dimensional metal, since the Na valence states strongly hybridize with the jellium bands in the present case. With decreasing Θ, the electron density at the Na—Na bond region becomes smaller, and the adatom electronic structure approaches that of an isolated adatom.

The lower panels of Fig. 4 show the corresponding difference charge defined by

$$\delta\rho(\mathbf{r},\Theta)=\rho(\mathbf{r},\Theta)-[\rho_{jet}(\mathbf{r})+\rho_{alk}(\mathbf{r},\Theta)] , \quad (4.1)$$

where $\rho(\mathbf{r},\Theta)$, $\rho_{jel}(\mathbf{r})$, and $\rho_{alk}(\mathbf{r},\Theta)$ denote the electron

charge densities of the Na-covered jellium, isolated jellium, and the unsupported Na layer, respectively. The definition is quite natural in elucidating the charge redistribution caused by the mutual interaction between the overlayer and substrate. By the definition, $\delta\rho(\mathbf{r},\Theta)$ satisfies the condition

$$\int d\mathbf{r}\,\delta\rho(\mathbf{r},\Theta)=0\ . \tag{4.2}$$

The characteristic features in $\delta\rho(\mathbf{r},\Theta)$ common to all the coverages are the buildup of the electron density at the interface of the jellium and Na layer and the corresponding charge depletions in the jellium and Na sides. The Θ dependence of the charge redistribution is discussed in detail in the following.

Figure 5 shows the contour maps of the difference charges for the five Na coverages on the same vertical-cut plane as in Fig. 4. The shaded and hatched areas designate the regions where $\delta\rho(\mathbf{r},\Theta)\geq 0.001$ a.u. (accumulation of the electron density) and $\delta\rho(\mathbf{r},\Theta)\leq -0.0005$ a.u. (depletion of the electron density), respectively. The dashed-dotted curves correspond to $\delta\rho(\mathbf{r},\Theta)=0$. The charge map for $\Theta=\frac{1}{5}$ bears a close resemblance to that of Li plus jellium given by Lang and Williams[20] for single-atom chemisorption, suggesting that the direct interaction among adatoms is negligibly small at $\Theta=\frac{1}{5}$. Hence, Fig. 5 traces the Θ dependence of the difference charge in the whole regime during monolayer formation. It is striking that the bond charge is formed between the jellium and adatom irrespective of Θ and that its contour (shaded area) and amplitude are almost unchanged throughout monolayer formation. Slight expansion (contraction) of its contour vertical (parallel) to the surface with increasing Θ is the only noticeable minor change. This may be interpreted as implying that the nature of the adatom-substrate bonding remains essentially un-

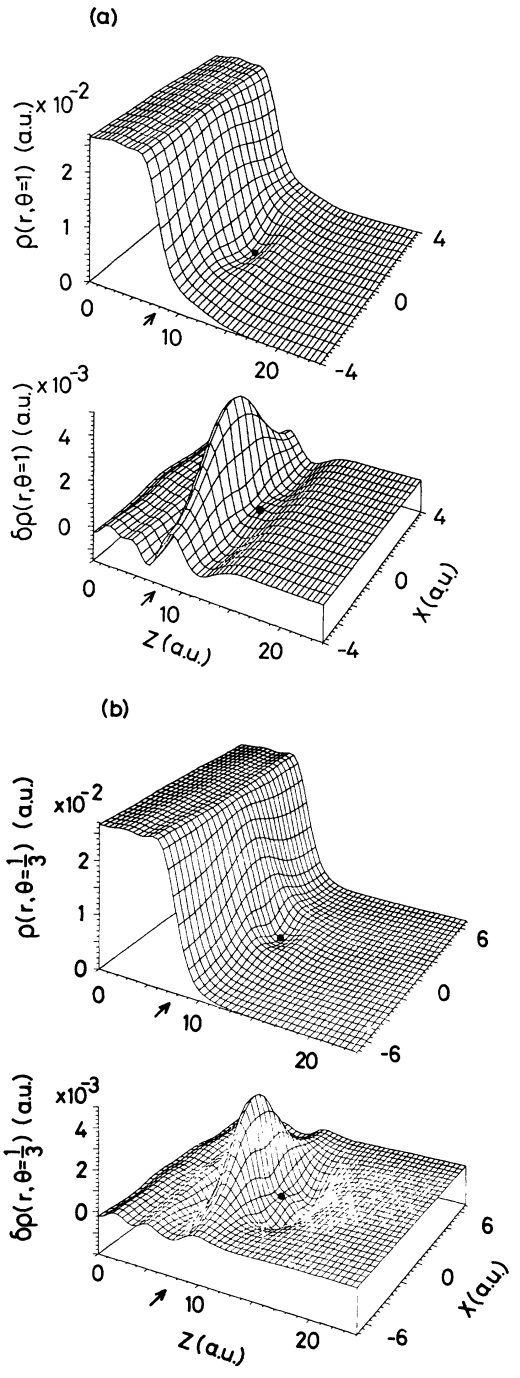

FIG. 4. Upper panels: calculated electron densities of the Na/jellium surfaces on a vertical-cut plane passing Na atoms at every interval of $a_{\parallel}$. The jellium edge and Na atoms are indicated by arrows and solid circles, respectively. Lower panels: corresponding difference charges defined by Eq. (4.1) on the same vertical-cut plane. (a) $\Theta=1$ and (b) $\Theta=\frac{1}{3}$.

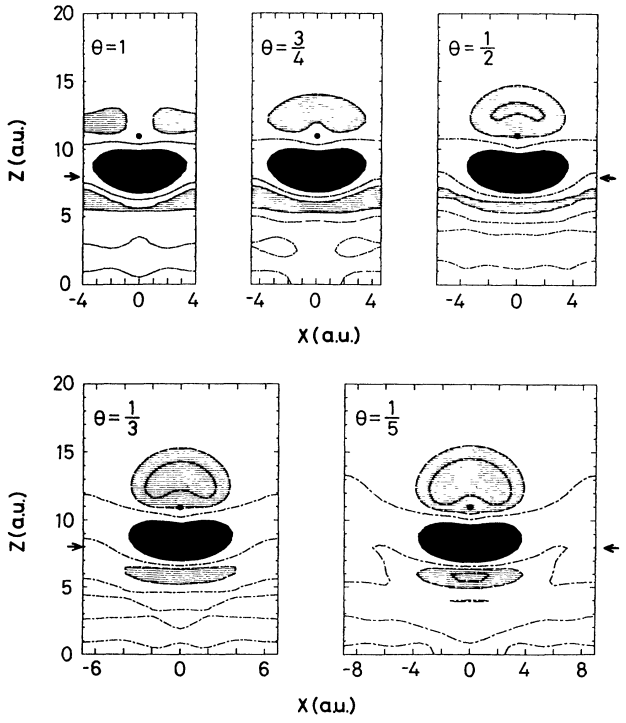

FIG. 5. Contour maps of the difference charge $\delta\rho(\mathbf{r},\Theta)$ for the Na/jellium surfaces on the same vertical-cut plane as in Fig. 4. The shaded and hatched areas indicate the regions where $\delta\rho(\mathbf{r},\Theta)\geq 0.001$ a.u. and $\delta\rho(\mathbf{r},\Theta)\leq -0.0005$ a.u., respectively. The dashed-dotted lines corresponds to $\delta\rho(\mathbf{r},\Theta)=0$.

changed during monolayer formation. On the other hand, the major Θ dependence exists in the hatched areas, from which electrons flow into the bond region. The kidney-shaped charge depletion on the vacuum side of Na becomes smaller with increasing Θ, and the center of gravity of the depletion region on the Na side moves from the outside of Na to the Na—Na bond region. At $\Theta=1$ the major depletion area in the Na side appears between neighboring Na adatoms at the expense of some bonding charge between Na—Na metallic bonds. On the other hand, the Θ dependence of the depletion region in the jellium side is not so drastic. However, it should be noted that the depletion in the substrate side is not small. Actually, as seen from Fig. 4, the deepest charge depletion appears in the jellium side rather than the Na side at $\Theta=1$. The above Θ dependence of the charge redistribution is far from the point-charge-transfer model assumed in the model analyses based on the Newns-Anderson Hamiltonian.[27–30]

The increase and decrease of the electron density in realistic calculations occur in the interface and vacuum sides of an adatom, respectively. Therefore, the depolarization field at adatom sites evaluated based on a classical point-charge-transfer model, Eq. (2.5), is not appropriate. Figure 6 shows the change in the electrostatic potential $\delta\varphi_{el}(\mathbf{r},\Theta)$ due to $\delta\rho(\mathbf{r},\Theta)$, i.e.,

$$\delta\varphi_{el}(\mathbf{r},\Theta)=\int d\mathbf{r}'\frac{\delta\rho(\mathbf{r}',\Theta)}{|\mathbf{r}-\mathbf{r}'|} \tag{4.3}$$

for $\Theta=\frac{1}{5}$, $\frac{1}{3}$, $\frac{1}{2}$ and 1 on the same vertical-cut plane as in Figs. 4 and 5. The electrostatic potential is surely lowered on the vacuum side of a Na adatom due to the dipole fields of adatoms, whereas it shows no appreciable downward shift with increasing Θ at a Na site. It should be noted that the adatom dipole field exists only on the vacuum side of adatoms. Owing to the efficient screening of the high-density jellium, $\delta\varphi_{el}(\mathbf{r},\Theta)$ created by a single adatom is of short range in the adatom plane. Therefore the increase in the adatom number does not result in the potential lowering in the plane; the calculated $\delta\varphi_{el}(\mathbf{r},\Theta)$ at a Na site as measured from the interior of the jellium are -0.40, -0.15, -0.14, and -0.24 eV for $\Theta=\frac{1}{5}$, $\frac{1}{3}$, $\frac{1}{2}$, and 1, respectively. To support this argument, we further show in Fig. 7 the calculated s part of the total adatom potential including Na core and exchange-correlation parts in addition to the electrostatic potential, which gives the site energy of an s-orbital in LCAO (linear combination of atomic orbitals) methods. R denotes the distance from a Na core, and the potential energy is measured from the bottom of the jellium potential. It is seen that the total s potential is remarkably independent of Θ within a Na atomic sphere from $\Theta=\frac{1}{5}$ to 1. Therefore one cannot expect a large depolarization shift of the adatom s level, which is typically assumed to be more than 1 eV in order to reproduce the Θ dependence of the adatomic dipole. As will be shown later, the depolarization shift of the adatom valence states below E_F is indeed absent in the present calculation.

Figure 8 shows the similar difference charge-contour maps of the Li/jellium systems at $\Theta=1$, $\frac{3}{4}$, and $\frac{1}{2}$. D_{as} is determined from the calculated total energy as 2.4, 2.5, and 2.6 a.u. for $\Theta=\frac{1}{2}$, $\frac{3}{4}$, and 1, respectively. It is seen that qualitative features of the charge redistribution are independent of the alkali-metal adspecies.

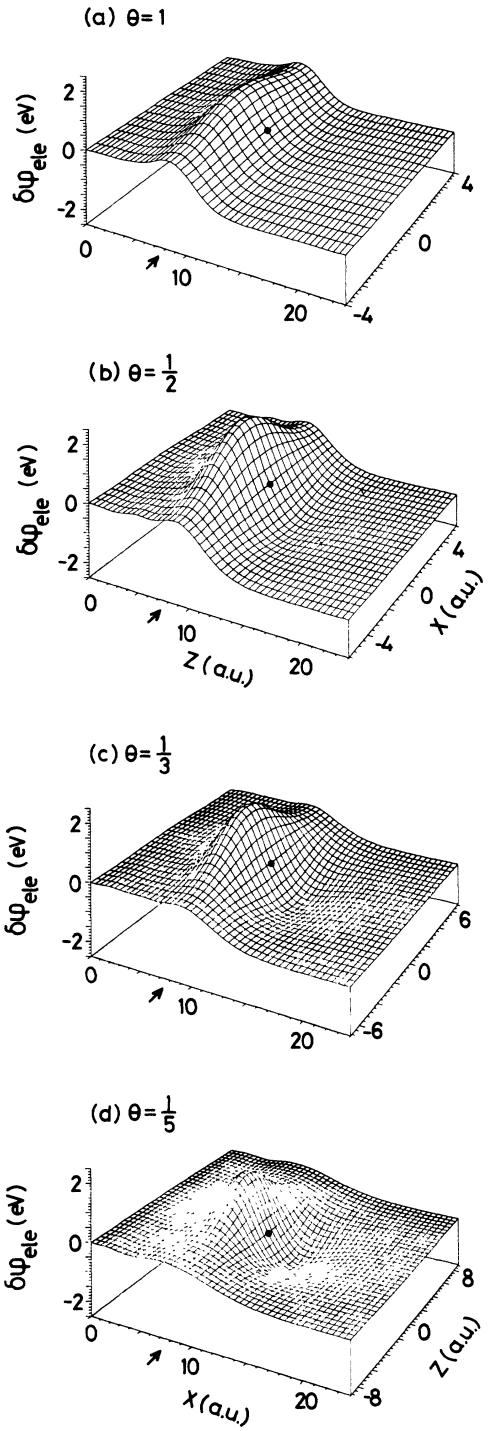

FIG. 6. The change in the electrostatic potential $\delta\varphi_{el}(\mathbf{r},\Theta)$ due to the charge redistribution $\delta\rho(\mathbf{r},\Theta)$ for the Na/jellium surfaces on the same vertical-cut plane as in Fig. 4. (a) $\Theta=1$, (b) $\Theta=\frac{1}{2}$, (c) $\Theta=\frac{1}{3}$, and (d) $\Theta=\frac{1}{5}$.

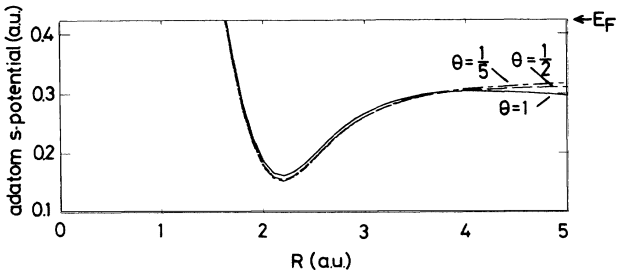

FIG. 7. The s part of the total adatom potential for a Na adatom on jellium. R denotes the distance from the Na core, and the origin of the potential energy is the bottom of the jellium potential.

B. Work-function change and adatom dipole moment

The work function of metal surfaces is defined as a minimum energy to remove electrons in metals to the vacuum. Within the local-density-functional theory, the potential barrier confining electrons in metals consists of the surface dipole layer (contribution of the electrostatic potential) and the exchange-correlation potential. The work-function change $\Delta\Phi(\Theta)$ of metals due to the alkali-metal adsorption originates from the change of the former due to the charge redistribution $\delta\rho(\mathbf{r},\Theta)$. From Fig. 6 one sees that the electrostatic potential change is almost constant in the vacuum region and interior of the jellium. $\delta\varphi_{\rm el}(\mathbf{r},\Theta)$ in the former is lower than that in the latter, indicating that the electrostatic potential barrier is reduced by the alkali-metal adsorption. The difference in $\delta\varphi_{\rm el}(\mathbf{r},\Theta)$ between the vacuum and interior of the jellium gives the work-function change $\Delta\Phi(\Theta)$. Equally, $\Delta\Phi(\Theta)$ is expressed as

$$\Delta\Phi(\Theta)=4\pi\int_0^{A_z/2} dz\, z\,\delta\rho_{\rm av}(z,\Theta)\ , \tag{4.4}$$

where $\delta\rho_{\rm av}(z,\Theta)$ denotes the planar average of the difference charge, Eq. (4.1). The work function of the system is also directly obtained as the vacuum level measured from the Fermi energy E_F. The two expressions should give the same value if the system is semi-infinite. Because of the use of the finite jellium slab, there is a small discrepancy between the two values. However, it is at most 0.05 eV and causes no problem in discussing the work-function change of an order of 0.1 eV. The results given in the following are based on Eq. (4.4). The induced dipole moment per an adatom, $d(\Theta)$, is related to the work-function change by

$$d(\Theta)=\frac{\Delta\Phi(\Theta)a_{\parallel}^2}{4\pi}\ . \tag{4.5}$$

The calculated work function and adatom dipole are shown as a function of Θ in Fig. 9 for the Na-covered high-density jellium surface. The outward dipole which reduces the work function monotonically decreases with increasing Θ. The origin of the outward dipole is the buildup of the electron density (bond charge) in the interface and the corresponding major depletion area in the vacuum side of Na shown in Fig. 5. Its monotonic decrease reflects the inward shift of the center of gravity of the depletion area on the Na side as well as the relative increase of the weight of the depletion area on the jellium side when Θ is increased. On account of the rapid decrease of the adatom dipole, the calculated work function deviates from its linear dependence on Θ, takes a minimum at about $\Theta=\frac{1}{2}$, and begins to rise toward a saturation value. The work function at $\Theta=1$ and 2.8 eV is close to that of N(001), 2.9 eV, which is calculated with a five-layer slab model following the same calculational scheme. The present jellium substrate might be the best to simulate the most closely packed Al(111) surface. For Al(111), Hohlfeld *et al.*[7] measured the work function as a function of Cs coverage. The atomic density corresponding to the minimum point was 0.2×10^{15} atoms/cm^2,

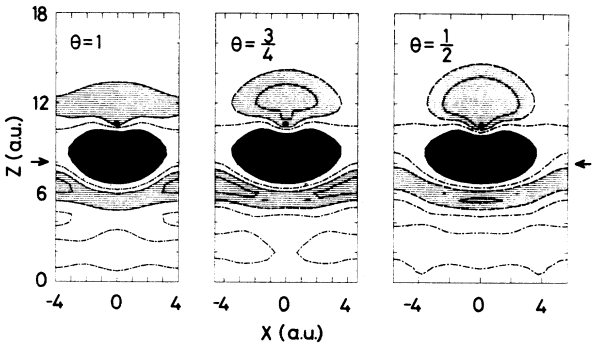

FIG. 8. Contour maps of the difference charge $\delta\rho(\mathbf{r},\Theta)$ for the Li/jellium surfaces on a vertical-cut plane passing Li adatoms at every interval of $a_{\parallel}$. The jellium edge and Li atoms are indicated by arrows and solid circles, respectively. The shaded and hatched areas indicate the regions where $\delta\rho(\mathbf{r},\Theta)\geq 0.001$ a.u. and $\delta\rho(\mathbf{r},\Theta)\leq -0.0005$ a.u., respectively. The dashed-dotted lines correspond to $\delta\rho(\mathbf{r},\Theta)=0$.

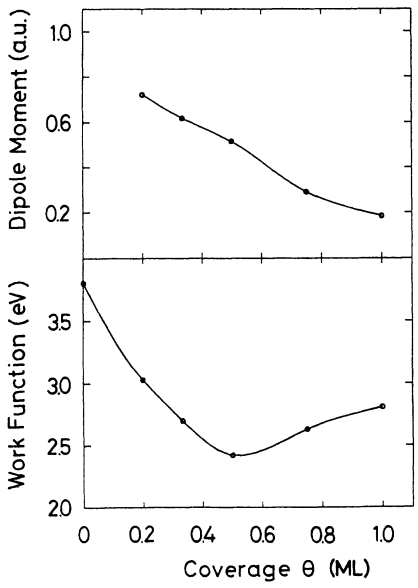

FIG. 9. The calculated work function and adatom dipole moment as a function of Θ on the Na/jellium surface.

which is somewhat smaller than the present value, 0.28×10^{15} atoms/cm^2, at $\Theta=\frac{1}{2}$. The difference may be attributed to a larger atomic size of Cs as compared with Na, since it leads to a larger adatom-adatom interaction at lower Θ. The above result shows that the widely observed characteristic variation of the work function with increasing Θ can be well reproduced, as far as the charge redistribution by the adatom-substrate interaction is described realistically by a first-principles method. Large relaxation of D_{as} (Ref. 29) and/or clustering among adatoms[30] are/is not essential for the appearance of the work-function minimum

In order to shed light on the origin of the rapid decrease of $d(\Theta)$ with increasing Θ, the calculated planar average of the charge redistribution $\delta\rho_{\rm av}(z,\Theta)$ is shown as a function of Θ in Fig. 10. Its asymmetry about the center plane of the bond charge at the Na-jellium interface is the origin of the outward dipole layer. It is seen that $\delta\rho_{\rm av}(z,\Theta)$ is quite different from a classical point-charge-transfer model assumed in the Newns-Anderson–model analysis. For the sake of quantitative discussions, let us define the effective dipole length $D_{\rm eff}(\Theta)$ as

$$D_{\rm eff}(\Theta)=2\int dz\, z\,\delta\rho_{\rm av}(z,\Theta)\Big/\int dz\,|\,\delta\rho_{\rm av}(z,\Theta)\,|\ . \tag{4.6}$$

For a classical dipole made of two positive and negative point charges, $D_{\rm eff}(\Theta)$ just gives the distance between the two charges. In the standard model analysis, $D_{\rm eff}(\Theta)$ is assumed constant and all of the Θ dependence of $d(\Theta)$ is attributed to a decrease in the transferred charge $Q(\Theta)$ with increasing Θ. However, $D_{\rm eff}(\Theta)$ actually depends significantly on Θ. The calculated $D_{\rm eff}(\Theta)$ are 2.4, 2.0, 1.8, and 1.5 a.u. for $\Theta=\frac{1}{5}$, $\frac{1}{3}$, $\frac{1}{2}$, and 1, respectively. This rapid contraction of $D_{\rm eff}(\Theta)$ comes from the inward shift of the depletion region on the Na side, and plays a crucial role in reproducing the rapid decrease of the adatom dipole necessary for the appearance of the work-function minimum.

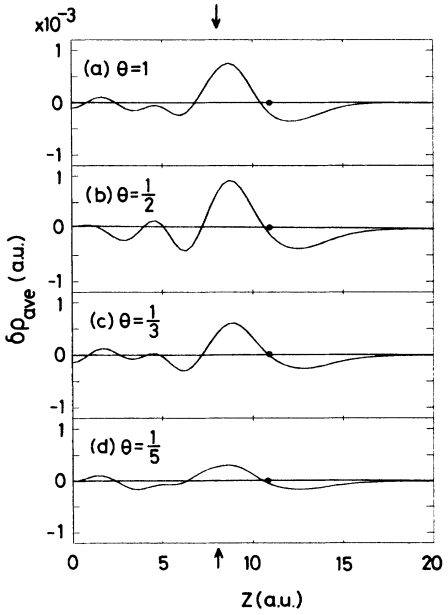

FIG. 10. The planar average of the difference charge $\delta\rho_{\rm av}(z,\Theta)$ for the Na/jellium surfaces. (a) $\Theta=1$, (b) $\Theta=\frac{1}{2}$, (c) $\Theta=\frac{1}{3}$, and (d) $\Theta=\frac{1}{5}$.

C. Adatom valence states

The discrete energy levels of an isolated alkali-metal atom are strongly modified by the interaction with the high-density metal substrate. The key point to be clarified is whether there is a large Θ dependence in the alkali-metal valence levels. For this purpose, we calculate the adatom-induced DOS, $\rho_\alpha(\varepsilon,\Theta)$ defined by

$$\rho_\alpha(\varepsilon,\Theta)=\int_R d\mathbf{r}\sum_i |\,\psi_i^\Theta(\mathbf{r})\,|^2\,\delta(\varepsilon-\varepsilon_i^\Theta) - \int_R d\mathbf{r}\sum_i |\,\psi_i^{\Theta=0}(\mathbf{r})\,|^2\,\delta(\varepsilon-\varepsilon_i^{\Theta=0})\ , \tag{4.7}$$

where ε_i^Θ and $\Psi_i^\Theta(\mathbf{r})$ are the energy and wave function of the one-electron state at coverage Θ, and the integration is done within a sphere of radius R (approximately the atomic radius of alkali-metal atoms) centered at an adatom site. The above definition coincides with that of Lang and Williams[20] used in the study of single-atom chemisorption on the jellium surface if R is sufficiently large. In the present study the maximum of R is limited by the condition that two spheres at neighboring adatom sites do not overlap. The calculated $\rho_a(\varepsilon,\Theta)$ is shown in Fig. 11 as a function of Θ. The origin of the energy is adjusted to E_F and the sphere radius R is chosen as 3.83 a.u. The qualitative aspect of the results is insensitive to the small difference of R. Due to the slab approximation for the jellium substrate, the continuum energy spectrum of a semi-infinite jellium in the surface-normal direction is replaced by discrete energy levels in the present case. As a result, the calculated $\rho_a(\varepsilon,\Theta)$ is modified even at the low-Θ limit from that of a single Na atom on the semi-infinite jellium given by Lang and Williams.[20] In particular, the interaction of the discrete jellium and adatom lev-

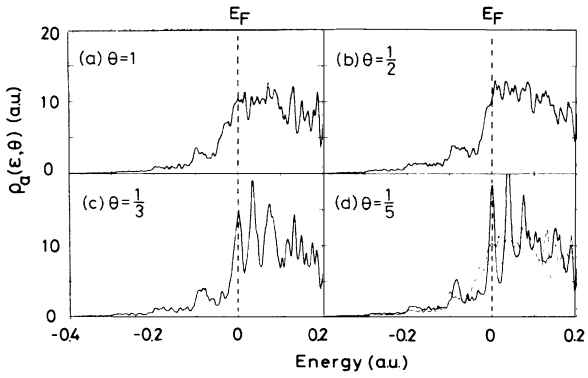

FIG. 11. The calculated adatom valence density of states $\rho_a(\varepsilon,\Theta)$ for the Na/jellium surfaces. The origin of the energy is adjusted to the Fermi level (E_F) for all the coverages. (a) $\Theta=1$, (b) $\Theta=\frac{1}{2}$, (c) $\Theta=\frac{1}{3}$, and (d) $\Theta=\frac{1}{5}$. For the sake of comparison, $\rho_a(\varepsilon,\Theta)$ at $\Theta=1$ is shown also in panel (d) by dashed lines.

els results in sharp spiky peaks at low Θ, which would disappear with semi-infinite substrates. Nevertheless, from the comparison of $\rho_a(\varepsilon,\Theta)$ at $\Theta=\frac{1}{5}$ and that for a single Na adatom on a semi-infinite jellium, one finds that they are essentially the same once the sharp spiky peaks in $\rho_a(\varepsilon,\Theta)$ at $\Theta=\frac{1}{5}$ are smeared out around the peak energies; smeared $\rho_a(\varepsilon,\Theta)$ would take a maximum value at ~ 1.5 eV above E_F.

With increasing Θ, discrete energy levels of an isolated Na adatom become broad bands by the overlap of neighboring adatom orbitals. Consequently, sharp peaks in $\rho_a(\varepsilon,\Theta)$ at lower Θ become broad structures. Except for this broadening of sharp peaks, no noticeable changes occur in $\rho_a(\varepsilon,\Theta)$ with increasing Θ. In fact, no downward shift of the adatom valence states was observed below E_F in the present calculation. In Fig. 11(d), $\rho_a(\varepsilon,\Theta)$ at $\Theta=1$ is shown by dashed lines for the sake of comparison with that at $\Theta=\frac{1}{5}$. The adatom dipole at $\Theta=\frac{1}{5}$ is more than 3 times larger than that at $\Theta=1$. However, the corresponding change in the occupation of adatom states is negligible, which is consistent with the fact that $\delta\varphi_{\rm el}(\mathbf{r},\Theta)$ at adatom sites is almost independent of Θ. Let us define the occupation of adatom valence states in the sphere $n_a^R(\Theta)$ by

$$n_a^R(\Theta)=\int_{\varepsilon\le E_F} d\varepsilon\,\rho_a(\varepsilon,\Theta)\ . \tag{4.8}$$

The calculated $n_a^R(\Theta)$ ($R=3.83$ a.u.) are 0.65, 0.61, 0.68, 0.62, and 0.63 electrons for $\Theta=\frac{1}{5}$, $\frac{1}{3}$, $\frac{1}{2}$, $\frac{3}{4}$, and 1, respectively. It may be concluded that $n_a^R(\Theta)$ is independent of Θ within small numerical errors. The quite small Θ dependence of the occupation of adatom valence states as compared with $d(\Theta)$ is in agreement with the recent MDS experiment of Woratschek *et al.*[11] Moreover, $n_a^R(\Theta)$ is ~ 0.01 electrons larger than the number of electrons within the same sphere calculated for the corresponding isolated Na monolayers $[n_{\rm iso}^R(\Theta)]$ regardless of Θ, implying that the adatom region is essentially neutral even at low Θ.

One possible mechanism which accounts for the increase and decrease of the electron density in the interface and vacuum sides of Na atoms is the polarization of a Na adatom by the mixing of the Na $3s$ and $3p_z$ states (intra-atomic polarization). In order to examine this effect, we next study partial DOS of Na adatoms as a function of Θ. For this purpose, the wave function $\psi_i^\Theta(\mathbf{r})$ is expanded within the sphere centered at an adatom into s, p, and higher-angular-momentum components. With the present calculational scheme, this is easily done by expanding plane-wave bases into spherical Bessel functions. Then the partial DOS of the lth ($l=s,p_x,p_z,\ldots$) component of the adatom valence state is defined as

$$\rho_a(\varepsilon,l,\Theta)=\int_R d\mathbf{r}\sum_i |\psi_{i,l}^\Theta(\mathbf{r})|^2\delta(\varepsilon-\varepsilon_i^\Theta) - \int_R d\mathbf{r}\sum_i |\psi_{i,l}^{\Theta=0}(\mathbf{r})|^2\delta(\varepsilon-\varepsilon_i^{\Theta=0})\ , \tag{4.9}$$

where $\psi_{i,l}^\Theta(\mathbf{r})$ denotes the lth component of $\psi_i^\Theta(\mathbf{r})$ in the sphere. The calculated s, p_x (p_y), and p_z partial DOS's of a Na adatom are shown in Figs. 12, 13, and 14 as a func-

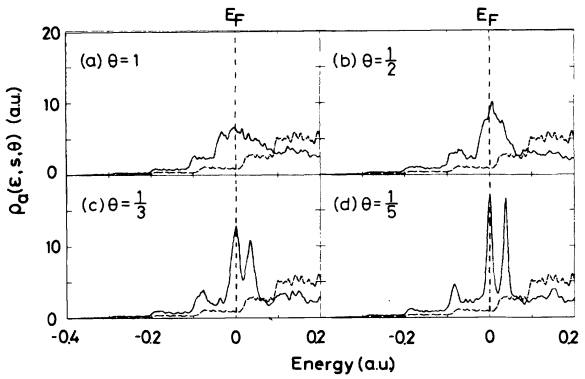

FIG. 12. The calculated s partial density of states of a Na adatom on the jellium surface. (a) $\Theta=1$, (b) $\Theta=\frac{1}{2}$, (c) $\Theta=\frac{1}{3}$, and (d) $\Theta=\frac{1}{5}$. The thick and dashed lines indicate the first and second terms of the right-hand side of Eq. (4.9), respectively.

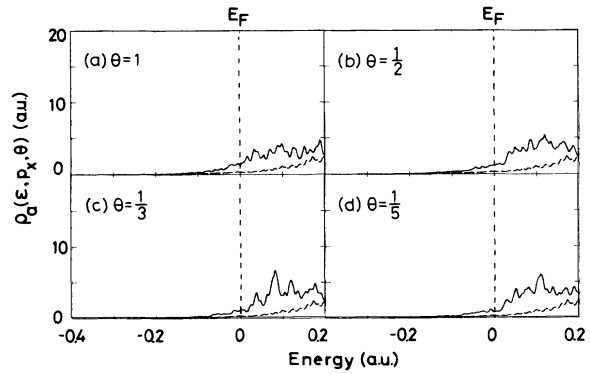

FIG. 13. The calculated p_x partial density of states of a Na adatom on the jellium surface. (a) $\Theta=1$, (b) $\Theta=\frac{1}{2}$, (c) $\Theta=\frac{1}{3}$, and (d) $\Theta=\frac{1}{5}$. The thick and dashed lines indicate the first and second terms of the right-hand side of Eq. (4.9), respectively.

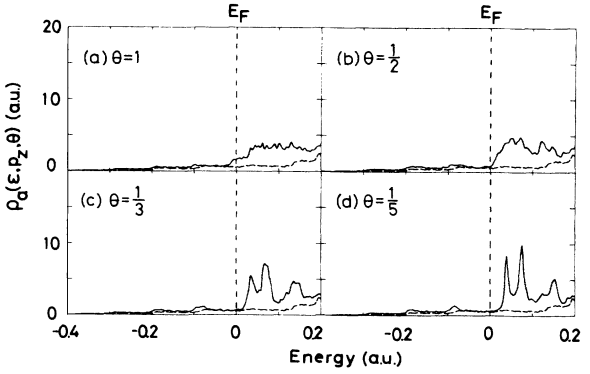

FIG. 14. The calculated p_z partial density of states of a Na adatom on the jellium surface. (a) $\Theta=1$, (b) $\Theta=\frac{1}{2}$, (c) $\Theta=\frac{1}{3}$, and (d) $\Theta=\frac{1}{5}$. The thick and dashed lines indicate the first and second terms of the right-hand side of Eq. (4.9), respectively.

tion of Θ, respectively. The sphere radius $R=3.83$ a.u. is the same as in Fig. 11. The thick and dashed curves indicate the first and second terms of the right-hand side of Eq. (4.9), and thus the lth partial DOS induced by Na is given by the difference of the thick and dashed curves. The spiky sharp peaks in the partial DOS grow into broad band structures with increasing Θ by the overlap of neighboring adatom orbitals. The important fact is that the Na-induced states below E_F mostly come from the $3s$ component of a Na adatom. It is seen from Fig. 14 that Na $3p_z$ is essentially located above E_F. [$\rho_a(\varepsilon,p_x,\Theta)$ is more broadened than $\rho_a(\varepsilon,p_z,\Theta)$ on account of the larger interaction with substrate states, and a small part of its tail is occupied even at low Θ.] This clearly shows that the redistribution of the electron density around a Na adatom, and therefore the adatom dipole is *not* caused by the mixing of the Na $3s$ and $3p_z$ states. On the other hand, $3s$ and $3p_z$ components admix strongly above E_F and give rise to outward-polarized states which have an antibonding character against the substrate, as will be discussed later.

In many of the electron-energy-loss–spectroscopy (EELS) experiments for alkali-metal-covered metal surfaces, an intensive loss peak characteristic of the alkali metal has been observed at higher Θ.[4,5,42–44] The valence structure of alkali-metal adatoms given in the above may suggest that the observed peak may be interpreted as being due to excitations from the partially filled s-like states to the unoccupied p_z-like states. The excitation satisfies the dipolar scattering condition[45] and thus should have a strong intensity. The present assignment is consistent with the conclusion in the model calculation of Ishida and Tsukada,[46] who studied the response function of the alkali-metal overlayer with the tight-binding Hamiltonian combined with the random-phase approximation (RPA).

In the calculation of Lang and Williams[20] for semi-infinite surfaces, the sharp peaks in $\rho_a(\varepsilon,\Theta)$ above E_F were smoothed out, and as a result $\rho_a(\varepsilon,\Theta)$ appeared as if it formed a single-peak structure with its center located ~ 1.5–2 eV above E_F. The single peak above E_F has been assigned as being due to the alkali-metal s state and considered evidence of the mostly empty alkali-metal s level. However, the above partial-DOS analysis of the alkali-metal valence states clarified that Na-induced states above E_F are contributed by the strongly hybridized states of Na $3s$ and $3p$ rather than the pure Na $3s$.

D. Bond-order density

The above analysis of the adatom valence state, which is found to show only a minor change as a function of Θ, is unexpected from Gurney's picture,[10] in which the adatom-substrate bond is assumed to change drastically from ionic to covalent with increasing Θ. In order to clarify the nature of the adatom-substrate bonding more directly, we study the bond-order density defined by

$$\beta_{as}(\varepsilon,\Theta)=\sum_i [\psi_i^{\Theta}(\mathbf{r}_1)]^*\psi_i^{\Theta}(\mathbf{r}_2)\delta(\varepsilon-\varepsilon_i)+\text{c.c.}\ , \qquad (4.10)$$

where $\mathbf{r}_1$ and $\mathbf{r}_2$ are taken at some point in the interior of the jellium and at the Na site, respectively. Figure 15 shows the calculated $\beta_{as}(\varepsilon,\Theta)$ of the Na-covered jellium surfaces as a function of Θ. Here, $\mathbf{r}_1$ is chosen at a point on a vertical axis passing through a Na adatom and 2 a.u. inside the jellium edge. The calculated results are insensitive to the position of $\mathbf{r}_1$ unless it is too far from the bond region. The positive and negative parts of $\beta_{as}(\varepsilon,\Theta)$ correspond to the bonding and antibonding states, respectively. Qualitative features of $\beta_{as}(\varepsilon,\Theta)$ are understood from Eq. (2.19), especially for the region below E_F. Its rapid change of sign at the B-A boundary near E_F may be interpreted as being characteristic of the off-diagonal Green function. However, it was assumed in the discussion in Sec. II that the overlayer states originate only from the alkali-metal s orbital. The calculated $\beta_{as}(\varepsilon,\Theta)$ above E_F is modified from Eq. (2.19) because of the existence of higher orbitals such as Na $3p$ and continuum states above the vacuum level. There is a strong antibonding peak slightly above E_F which becomes sharper with decreasing Θ. The origin of the peak is the outward-polarized orbital made by strong mixing of the Na $3s$ and $3p_z$ components.

At $\Theta=\frac{1}{5}$, the B-A boundary is very close to E_F, indicating a formation of a metallic covalent bond by the maximum use of the bonding states. The buildup of the electron density at the interface of the jellium and Na shown in Fig. 5 is a natural consequence of this covalency. With increasing Θ, E_F slightly moves into the antibonding region. The bond order of the adatom-substrate bond is defined by

$$B_{as}(\Theta)=\int_{\varepsilon\le E_F} d\varepsilon\,\beta_{as}(\varepsilon,\Theta)\ . \qquad (4.11)$$

The calculated $B_{as}(\Theta)$ are 2.1×10^{-3}, 2.0×10^{-3}, 1.8×10^{-3}, and 1.6×10^{-3} a.u. for $\Theta=\frac{1}{5}$, $\frac{1}{2}$, $\frac{3}{4}$, and 1, respectively. The decrease of $B_{as}(\Theta)$ with increasing Θ implies weakening of the adatom-substrate bond, which is in accord with the small outward relaxation and decrease in a stretching frequency of a Na adatom with increasing Θ. The weakening of the adatom-substrate bond is more directly demonstrated from adatom binding energies. The adsorption energies of a Na adatom calculated as the total energy of the Na/jellium minus those of the bare jellium and unsupported Na layer are 1.5, 1.3, 1.1, 0.9, and

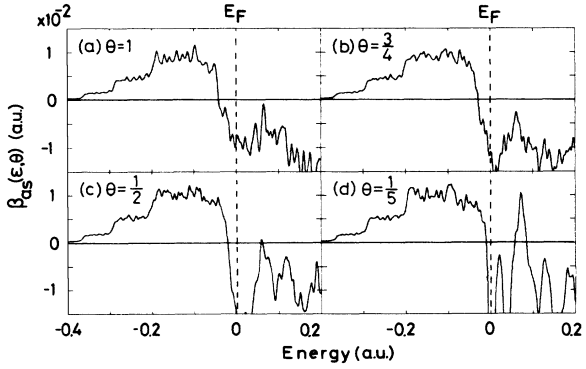

FIG. 15. The calculated bond-order density of the Na—jellium bond. (a) $\Theta=1$, (b) $\Theta=\frac{3}{4}$, (c) $\Theta=\frac{1}{2}$, and (d) $\Theta=\frac{1}{5}$.

0.7 eV for $\Theta=\frac{1}{5}, \frac{1}{3}, \frac{1}{2}, \frac{3}{4}$, and 1, respectively. Experimentally, such a rapid decrease of the adatom binding energy with increasing Θ has been known since the pioneering work of Taylor and Langmuir.[2] It is seen that the Θ dependence of $B_{as}(\Theta)$ is smaller than that of the Na binding energy. The definition of $\beta_{as}(\varepsilon,\Theta)$ includes only the amplitude of one-electron wave functions at a particular point $\mathbf{r}_1$ in the jellium, and takes no account of the Θ dependence of the bond region. Since the bond area per Na adatom diminishes as Θ^{-1} with increasing Θ, it may be natural that $B_{as}(\Theta)$ underestimates the weakening of the adatom-substrate bond.

The above result for the bond-order density is not in accord with Gurney's picture on the following points: (i) If the s resonance is primarily located above E_F at low Θ, E_F should be located inside the bonding region in $\beta_{as}(\varepsilon,\Theta)$, since the lower and upper halves of the s resonance may correspond to the bonding and antibonding regions, respectively; however, in the present calculation the B-A boundary coincides with E_F even at $\Theta=\frac{1}{5}$. (ii) If the adatom-substrate bonding changes from ionic to covalent, the bond order $B_{as}(\Theta)$, which is the measure of covalency, should increase with increasing Θ, while $B_{as}(\Theta)$ decreases with Θ in the present calculation.

The weakening of the adatom-substrate bond with increasing Θ is partly due to the corresponding strengthening of neighboring Na—Na bonds and formation of the Na $3s$ band. Its qualitative explanation is given schematically in Fig. 16. As was shown above, when two adatoms are separated enough, each atom can form a strong metallic adatom-substrate bond by the maximum use of bonding states formed by hybridization of the substrate states and adatom orbital φ_1 (or φ_2) [Fig. 16(a)]. On the other hand, with the decreasing adatom-adatom distance, the two adatom orbitals φ_1 and φ_2 split into bonding $[m_1=(\varphi_1+\varphi_2)/\sqrt{2}]$ and antibonding $[m_2=(\varphi_1-\varphi_2)/\sqrt{2}]$ molecular orbitals. When they interact with substrate states, the B-A boundaries of the m_1 and m_2 resonances in the m_i-substrate bond-order density may be located below and above E_F, respectively. In this case, from the viewpoint of adatom-substrate bonding, part of antibonding states is occupied for m_1, while part of bonding states is unoccupied for m_2 [Fig. 16(b)]. (m_1 and m_2 correspond to the lower and upper parts of the Na $3s$ band in a real overlayer, respectively.) Therefore, the bond order of the adatom-substrate bond per one adatom should become smaller, which then results in the weaker adatom-substrate bond at higher Θ.

Figure 17 shows the calculated bond-order density of the nearest Na—Na bond, $\beta_{aa}(\varepsilon,\Theta)$, as a function of Θ, which is computed by Eq. (4.10) with $\mathbf{r}_1$ and $\mathbf{r}_2$ taken at neighboring Na sites. By the indirect interaction of neighboring Na atoms through the substrate, $\beta_{aa}(\varepsilon,\Theta)$ shows oscillatory behavior as a function of ε for lower Θ. The Na—Na bond orders defined in the same way as Eq. (4.11) are 8.0×10^{-6}, 8.1×10^{-5}, 1.2×10^{-4}, and 1.8×10^{-4} a.u. for $\Theta=\frac{1}{5}, \frac{1}{2}, \frac{3}{4}$, and 1, respectively. The increase of the Na—Na bond order reflects larger adatom-adatom interaction with increasing Θ by the direct overlap of neighboring adatom orbitals. At $\Theta=1$ the direct interaction among adatoms surpasses the indirect one, and the calculated $\beta_{aa}(\varepsilon,\Theta)$ at $\Theta=1$ keeps a positive sign (bonding states) in most of the region below E_F. An important observation is that its bonding-antibonding boundary coincides fairly well with E_F just as in the case of an isolated Na layer. Even for $\beta_{aa}(\varepsilon,\Theta)$ at lower Θ, one notices a rapid change of its sign near E_F. This may imply that Na valence states are not influenced very much by a high-density jellium substrate even at low Θ, which is consistent with the result that the adatom region is essentially neutral irrespective of Θ.

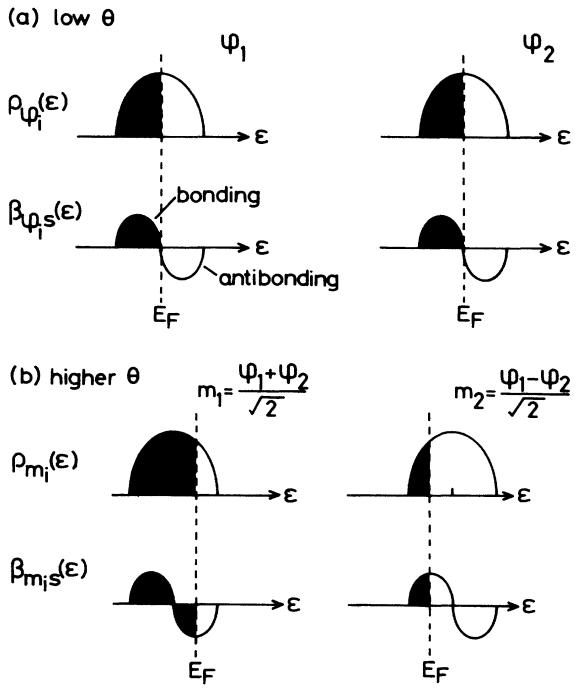

FIG. 16. Schematical illustration of the electronic structures of two adatoms when the overlap of two adatoms orbitals is (a) small and (b) large. $\rho_{\varphi_i}(\varepsilon)$ [$\rho_{m_i}(\varepsilon)$] denotes the state density of the φ_i resonance (m_i resonance), and $\beta_{\varphi_i s}(\varepsilon)$ [$\beta_{m_i s}(\varepsilon)$] denotes the φ_i-substrate (m_i-substrate) bond-order density as a function of the one-electron energy.

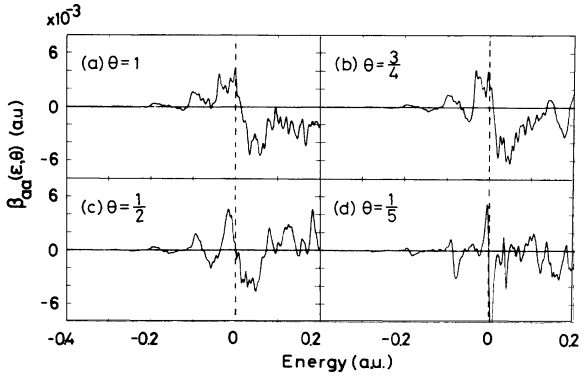

FIG. 17. The calculated bond-order density of the nearest Na—Na bond. (a) $\Theta=1$, (b) $\Theta=\frac{3}{4}$, (c) $\Theta=\frac{1}{2}$, and (d) $\Theta=\frac{1}{5}$.

E. Dipole density

Now let us proceed to the important problem about the origin of the adatom dipole. It is seen from Fig. 5 that the major charge-redistribution region due to the alkali-metal adsorption is localized around adatoms. If one takes a sphere with radius R centered at an adatom site, the dipole density within the sphere mostly comes from the crossterm of the s and p_z components of one-electron wave functions. Therefore the dipole density within the sphere $\mu(\varepsilon,\Theta)$ is calculated as

$$\mu(\varepsilon,\Theta)=\sum_i \int_R d\mathbf{r}\, z[\psi^{\Theta}_{i,s}(\mathbf{r})]^* \psi^{\Theta}_{i,p_z}(\mathbf{r})\delta(\varepsilon-\varepsilon_i^{\Theta})+\text{c.c.} \tag{4.12}$$

Figure 18 shows the calculated $\mu(\varepsilon,\Theta)$ of the Na-covered jellium surfaces as a function of Θ, where the sphere radius R is 3.83 a.u. Its positive sign corresponds to the inward polarization of the one-electron wave function (outward dipole). The dashed curves in the figure represent $\mu(\varepsilon,\Theta)$ at $\Theta=0$ calculated within the same sphere for the bare jellium surface. Therefore the difference between the solid and dashed curves contributes to the alkali-metal-induced dipole which lowers the work function [see Eq. (2.8)]. The induced dipoles within the sphere calculated by integrating the difference up to E_F are 0.34, 0.30, 0.18, and 0.12 a.u. for $\Theta=\frac{1}{5}$, $\frac{1}{2}$, $\frac{3}{4}$, and 1, respectively, which reproduces the rapid decrease of the adatom dipole with increasing Θ. Although the induced dipole within the sphere is less than half of the total adatom dipole shown in Fig. 9, one can obtain larger absolute values by increasing the sphere radius.

There is a qualitative difference in $\mu(\varepsilon,\Theta)$ between finite and zero Θ. The positive sign of $\mu(\varepsilon,\Theta)$ at $\Theta=0$ below the vacuum level (the work function of the jellium is 3.8 eV) means attenuation of one-electron wave functions into the vacuum region, which is seen as its inward polarization within the sphere. Its sudden drop at the vacuum level comes from the corresponding change of the dipole matrix elements On the other hand, $\mu(\varepsilon,\Theta)$ for a finite Θ shows quite different behaviors as a function of ε. Its sign changes rapidly near the Fermi level E_F. It is seen from the definition (4.12) that the negative sharp peaks above E_F indicate the strong mixing of the s and p_z components of wave functions. As shown before, these correspond to outward-polarized antibonding states mainly contributed by the Na $3s$ and $3p_z$ orbitals. The positive part in $\mu(\varepsilon,\Theta)$ below E_F designates the inward polarization of the one-electron states, which thus results in the buildup of the electron density in the interface (bond charge) shown in Fig. 5. By comparing Figs. 15 and 18, one finds a close similarity between the bond-order and dipole densities. The small deviation of the positive-negative boundary from E_F as well as broadening of the peaks above E_F with increasing Θ are common characteristic features observed both in the dipole and bond-order densities.

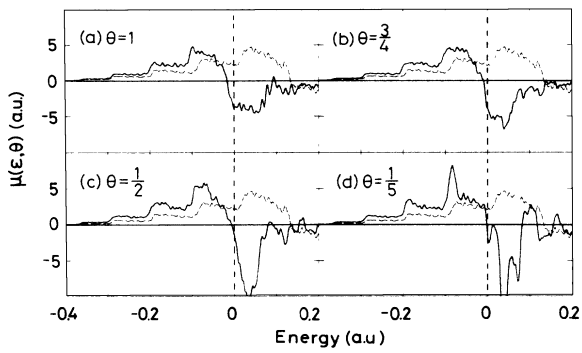

FIG. 18. The calculated dipole density within a sphere centered at a Na site on the Na/jellium surfaces. (a) $\Theta=1$, (b) $\Theta=\frac{3}{4}$, (c) $\Theta=\frac{1}{2}$, and (d) $\Theta=\frac{1}{5}$. The dashed lines in panels (a)–(d) show the dipole density of the bare jellium surface ($\Theta=0$).

In the present first-principles calculation there are no basis functions for the overlayer and substrate states as used in the discussions of Sec. II, so the adatom-induced dipole cannot be uniquely divided into the charge-transfer and hybridization terms. However, as discussed in Sec. II, the close similarity between the dipole and bond-order densities, as well as their characteristic energy dependence, strongly suggests that the adatom-induced dipole dominantly originates from the hybridization rather than the charge transfer. The fact that the buildup of the electron density which is responsible for the adatom dipole appears at the interface as a *covalent* bond charge supports the crucial role of the adatom-substrate hybridization term to the induced dipole. It was shown in the analysis of the partial DOS that the Na-induced p_z states are primarily located above E_F. Therefore, from the definition Eq. (4.12) [Eq. (4.12) extracts the dipole density coming from hybridization of the s and p_z components of wave functions], it may be quite natural to interpret that the adatom-induced dipole is caused by the polarization of an adatom due to hybridization of the partially filled Na $3s$ states and the p_z components of the substrate wave functions within the sphere.

F. On the Θ dependence of the adatom dipole

Negligibly small depolarization shifts of adatom valence states below E_F as well as the above analysis of bond-order and dipole densities clearly demonstrated that the adatom dipole cannot be explained in terms of the conventional Θ-dependent charge transfer. The Θ dependence of the adatom dipole should instead be attributed to the off-diagonal hybridization term, reflecting the strong interaction of the adatom and substrate metal [see Eq. (2.14)]. Then how should one interpret a rapid decrease of the dipole moment with increasing Θ, which is correctly reproduced in the present calculation? One reason is the weakening of the adatom-substrate bonding ($\propto \langle C^{\dagger}_{\alpha} C_{\beta} \rangle$), as exemplified by $B_{as}(\Theta)$ as well as adatom binding energies. The Na binding energy at $\Theta=1$ is $\sim 50\%$ of the corresponding one at $\Theta=\frac{1}{5}$. Secondly, the dipole matrix element $\mu_{\beta\alpha}$ in Eq. (2.14) may become significantly smaller with increasing Θ for the following reason: With increasing Θ, the weight of $|\varphi_a(\mathbf{r})|^2$ in the Na—Na bond region becomes larger at the expense of

that in vacuum sides, and as a result the major depletion area in the hybridization density

$$\sum_{\alpha\beta} \langle C_\alpha^\dagger C_\beta \rangle [\varphi_a(\mathbf{r})]^* \varphi_\beta(\mathbf{r}) + \text{c.c.}$$

moves from outside of a Na adatom to the Na—Na bond region. This effect appears as a rapid decrease of the effective dipole distance $D_{\text{eff}}(\Theta)$. The calculated $D_{\text{eff}}(\Theta)$ at $\Theta=1$ is $\sim 60\%$ of that at $\Theta=\frac{1}{5}$. If the above two effects are naively multiplied, the adatom dipole at $\Theta=1$ is estimated as $\sim 30\%$ (0.5×0.6) of that at $\Theta=\frac{1}{5}$, which is in agreement with the calculated ones.

V. SUMMARY AND CONCLUSION

In 1935, Gurney[10] proposed a simple picture which explains a large dipole of alkali-metal adatoms on metal surfaces and its rapid decrease with increasing coverage (Θ). He attributed the adatom dipole to ionicity of adatoms, and its subsequent decrease to adatom neutralization due to the downward shift of the adatom s resonance. This physically appealing picture has been widely accepted for more than half a century as a basic concept in the alkali-metal adsorption. Recently, there appeared several works which threw a doubt on this simplified view from both experimental and theoretical sides.[11–14] The purpose of the present study was to elucidate the electronic structure of the alkali-metal adatom as a function of Θ by a first-principles method and to help reestablish a more correct picture for alkali-metal adsorption.

The present calculation was based on the local-density-functional theory combined with the norm-conserving pseudopotential and plane-wave basis set. We used a jellium slab with $r_s=2.1$ a.u. to represent high-density metal substrates, and alkali-metal adatoms were assumed to form a square lattice whose lattice constant diminishes as $\Theta^{-1/2}$ with increasing Θ. The calculated work function reproduced its rapid lowering at initial Θ and a subsequent minimum very well. However, the charge redistribution due to the interaction of the adatom and substrate deviated far from the point-charge-transfer model, and the change in the electrostatic potential at adatom sites was found remarkably independent of Θ. Accordingly, the calculated adatom valence DOS showed no downward shift with increasing Θ. The adatom region was found essentially neutral irrespective of Θ. In order to clarify the nature of the adatom-substrate bond and adatom dipole more directly, the bond-order and dipole densities were calculated. It was shown that the adatom-substrate bond has strong covalency even at low Θ by the maximum use of bonding states. The calculated dipole density showed a close similarity to the bond-order density, which, together with the discussion in Sec. II, implied that the adatom polarization due to strong hybridization of the adatom and substrate states plays an significant role to the adatom dipole even at low Θ. The Θ dependence of the adatom dipole was attributed to a weakening of covalency in the adatom-substrate bond as well as a rapid decrease in the dipole matrix elements with increasing Θ.

The discussions on the dipole in Sec. II might give the reader an impression that which of the hybridization and charge transfer is dominant in the total adatom dipole is not physically so meaningful, since to divide the dipole into the two contributions depends on the basis functions for adatom and substrate states. However, it should be noted that the concept like the adatom s resonance and its bonding-antibonding boundary is a complete physical entity, which has nothing to do with a specific choice of the basis functions. As far as the basis functions are chosen so that they may be physically meaningful (for example, an s orbital located artificially on the vacuum side of an adatom should not be called the *alkali-metal* s orbital), we believe that our assignment of the adatom dipole to the adatom-substrate hybridization rather than the adatom ionization is a unique one that can explain all of the calculated results in a consistent way. In this regard, it should be emphasized that the present calculation is exact within the local-density-functional theory and thus the results themselves are free from the problem of interpretation. The new picture of alkali-metal adsorption presented in the present work is further supported by recent experimental works,[11–13] which cast doubt on the essence of Gurney's classical picture, such as the direct relationship between the adatom dipole and ionicity and the depolarization shift of adatom levels with increasing Θ.

ACKNOWLEDGMENTS

The author is grateful to Professor K. Terakura for valuable discussions and critical reading of the manuscript. The numerical calculations were done at the computer centers of University of Tokyo, Institute for Solid State Physics, and Institute for Molecular Science. This work was partially supported by a Grant-in-Aid for Scientific Research on Priority Areas by the Ministry of the Education, Science and Culture.

[1] K. H. Kingdon and I. Langmuir, Phys. Rev. **21**, 380 (1923).
[2] J. B. Taylor and I. Langmuir, Phys. Rev. **44**, 423 (1983).
[3] For example, J. P. Muscat and D. M. Newns, Prog. Surf. Sci. **9**, 1 (1978); N. D. Lang, in *Theory of the Inhomogeneous Electron Gas* edited by S. Lundqvist and N. H. March (Plenum, New York, 1983).
[4] T. Aruga, H. Tochihara, and Y. Murata, Phys. Rev. B **34**, 8237 (1986).
[5] J. Cousty, R. Riwan, and P. Soukiassian, J. Phys. (Paris) **46**, 1693 (1985).
[6] G. S. Tompa, M. Seidl, W. C. Ermler, and W. E. Carr, Surf. Sci. **185**, L453 (1987).
[7] A. Hohlfeld, M. Šunjić, and K. Horn, J. Vac. Sci. Technol. A **5**, 679 (1987); J. Paul, *ibid.* **5**, 664 (1987).
[8] D. Heskett, K.-H. Frank, E. E. Koch, and H.-J. Freund, Phys. Rev. B **36**, 1276 (1987).
[9] H. Tochihara, Surf. Sci. **126**, 523 (1983); T. Aruga, H. Tochihara, and Y. Murata, Phys. Rev. Lett. **53**, 372 (1984); E.

M. Oellig and R. Miranda, Surf. Sci. **177**, L947 (1986).
[10]R. W. Gurney, Phys. Rev. **47**, 479 (1935).
[11]B. Woratschek, W. Sesselmann, J. Küppers, G. Ertl, and H. Haberland, Phys. Rev. Lett. **55**, 1231 (1985).
[12]P. Soukiassian, R. Riwan, J. Lecante, E. Wimmer, S. R. Chubb, and A. J. Freeman, Phys. Rev. B **31**, 4911 (1985).
[13]H. Tochihara, M. Kubota, M. Miyano, and Y. Murata, Surf. Sci. **158**, 497 (1985).
[14]E. Wimmer, A. J. Freeman, J. R. Hiskes, and A. M. Karo, Phys. Rev. B **28**, 3074 (1983).
[15]H. Ishida and K. Terakura, Phys. Rev. B **36**, 4510 (1987).
[16]H. Ishida, N. Shima, and M. Tsukada, Phys. Rev. B **32**, 6246 (1985); H. Ishida, K. Terakura, and M. Tsukada, Solid State Commun. **59**, 365 (1986).
[17]S. R. Chubb, E. Wimmer, A. J. Freeman, J. R. Hiskes, and A. M. Karo, Phys. Rev. B **36**, 4112 (1987).
[18]G. A. Benesh, H. Krakauer, U. E. Ellis, and M. Posternak, Surf. Sci. **104**, 599 (1981).
[19]P. J. Feibelman and D. R. Hamann, Phys. Rev. Lett. **52**, 61 (1984); Surf. Sci. **149**, 48 (1985).
[20]N. D. Lang and A. R. Williams, Phys. Rev. B **18**, 615 (1978); **16**, 2408 (1977).
[21]N. D. Lang, Phys. Rev. B **4**, 4234 (1971).
[22]P. A. Serena, J. M. Soler, N. Garcia, and I. P. Batra, Phys. Rev. B **36**, 3452 (1987).
[23]C. A. Nicolaides, and A. N. Andriotis, Int. J. Quantum Chem. **23**, 561 (1983).
[24]P. A. Serena and N. Garcia, Surf. Sci. **189/190**, 232 (1987).
[25]W. Ning, C. Kailai, and W. Dingsheng, Phys. Rev. Lett. **56**, 2759 (1986); R. Wu, K. Chen, D. Wang, and N. Wang, Phys. Rev. B **38**, 3180 (1988).
[26]This observation is based on our first-principles electronic-structure calculation for Al/Na(001) at $\Theta=\frac{1}{2}$ [in units of Na(001) layers], where the distance between nearest-neighbor Al adatoms is 10.8 a.u. The calculated work function, 2.9 eV, of the five-layer Na(001) film increased to 4.1 eV by the Al adsorption.
[27]J. P. Muscat and D. M. Newns, Solid State Commun. **11**, 737 (1972).
[28]J. P. Muscat and D. M. Newns, J. Phys. C **7**, 2630 (1974).
[29]J. P. Muscat and I. P. Batra, Phys. Rev. B **34**, 2889 (1986).
[30]H. Ishida, N. Shima, and M. Tsukuda, Surf. Sci. **158**, 438 (1985).
[31]L. D. Schmidt and R. J. Gomer, J. Chem. Phys. **45**, 1605 (1966).
[32]A. J. Benett, J. Chem. Phys. **49**, 1340 (1968).
[33]P. W. Anderson, Phys. Rev. **124**, 41 (1961).
[34]D. M. Newns, Phys. Rev. **178**, 1123 (1969).
[35]A. C. Hewson and D. M. Newns, Jpn. J. Appl. Phys. Suppl. **2**, 121 (1974).
[36]See, for example, K. Terakura, J. Phys. F **7**, 1773 (1977).
[37]P. Hohenberg and W. Kohn, Phys. Rev. **136**, B864 (1964).
[38]W. Kohn and L. J. Sham, Phys. Rev. **140**, A1133 (1965).
[39]G. B. Bachelet, D. R. Hamann, and M. Schlüter, Phys. Rev. B **26**, 4199 (1982).
[40]G. Lehmann and M. Taut, Phys. Status Solidi B **54**, 469 (1972).
[41]N. D. Lang and W. Kohn, Phys. Rev. B **1**, 4555 (1970).
[42]A. U. MacRae, K. Muller, J. J. Lander, J. Morrison, and J. C. Phillips, Phys. Rev. Lett. **22**, 1048 (1969).
[43]S. Thomas and T. W. Haas, Solid State Commun. **11**, 193 (1972); S. Andersson and U. Jostell, Surf. Sci. **46**, 625 (1974); S. Å. Lindgren and L. Walldén, Phys. Rev. B **22**, 5969 (1980).
[44]U. Jostell, Surf. Sci. **82**, 333 (1979).
[45]For example, H. Ibach and D. L. Mills, *Electron Energy Loss Spectroscopy and Surface Vibrations* (Academic, New York, 1982).
[46]H. Ishida and M. Tsukada, Surf. Sci. **169**,225 (1986).

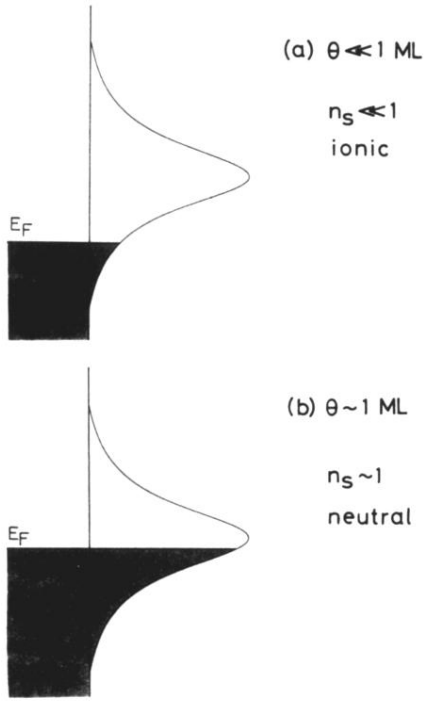

FIG. 1. Schematic energy diagram of the alkali-metal adatom *s* resonance originally proposed by Gurney (Ref. 10) at (a) the low-Θ and (b) the high-Θ limit. ML denotes monolayers.